SCIENTIFIC REPORTS

OPEN

SUBJECT AREAS:
NANOPHOTONICS AND PLASMONICS
INTEGRATED OPTICS
NANOSCALE DEVICES
SUB-WAVELENGTH OPTICS

Received
6 February 2013

Accepted
13 May 2013

Published
3 June 2013

Correspondence and requests for materials should be addressed to Z.L. (z_li@pku.edu.cn) or Q.H.G. (qhgong@pku.edu.cn)

A submicron broadband surface-plasmon-polariton unidirectional coupler

Huimin Liao[1], Zhi Li[1], Jianjun Chen[1,2,3], Xiang Zhang[1], Song Yue[1] & Qihuang Gong[1]

[1]State Key Laboratory for Mesoscopic Physics and Department of Physics, Peking University, Beijing 100871, China, [2]State Key Laboratory of Information Photonics and Optical Communications, Beijing University of Posts and Telecommunications, Beijing 100876, China, [3]School of Science, Beijing University of Posts and Telecommunications, Beijing 100876, China.

The manipulation of light propagation is a basic subject in optics and has many important applications. With the development of nano-optics, this area has been downscaled to wavelength or even subwavelength scales. One of the most efficient ways to control light propagation is to exploit interference effects. Here, by manipulating the interference between two nanogrooves on a metal surface, we realize a submicron broadband surface-plasmon-polariton (SPP) unidirectional coupler. More importantly, we find an anomalous bandwidth shrinking behavior in the proposed SPP unidirectional coupler as the groove separation is down to a subwavelength scale of one-quarter of the SPP wavelength. This abnormal behavior is well explained by considering the contribution of the near-field quasi-cylindrical waves in addition to the interference of propagating SPPs and the dispersion effects of individual grooves. Such near-field effects provide new opportunities for the design of ultracompact optical devices.

The manipulation of light propagation is a basic subject in optics and has many important applications. One of the most efficient ways to control light propagation is to exploit interference effects[1]. By regulating the amplitudes, initial phases and separations of a series of light sources, the propagation direction and field distribution of an optical field can be well manipulated. This strategy is widely employed in many aspects ranging from the classical gratings[1], radio-wave antennas[2] to the more recently developed research area of nano-optics, such as optical antennas[3–5], surface–plasmon-polariton (SPP) directional excitation[6,7] and focusing[8,9], and so on[10].

Traditionally, the bandwidth of an interference component is roughly inversely correlated to the interference length when the interfering sources have no dispersion effects, because the interferences are mainly determined by the propagating phase shifts between different sources in this case. Thus, a smaller separation of interfering sources usually gives a broader device's working bandwidth. Such broadband nature is highly preferred because it can greatly extend the application scope of a real optical component. In the paper, a submicron broadband SPP unidirectional coupler is proposed and experimentally demonstrated. First, the interference between two nanogrooves on a metal surface is manipulated to realize unidirectional launching of SPPs with high extinction ratio and high excitation efficiency. Then, by decreasing the groove separation to three-quarter of the SPP wavelength, a broad bandwidth of roughly 200 nm with high extinction ratios of $\geq$10 dB is successfully achieved. However, further reduction of the groove separation to one-quarter of the SPP wavelength results in an abnormal shrinking in the bandwidth. Such an anomalous phenomenon cannot be simply explained by taking into account the interference of the propagating SPPs and the dispersion effects of individual grooves. It is found that the near-field quasi-cylindrical waves (CWs) give important contributions to the abnormal bandwidth shrinking. This is the first time significant influence of the CW component on the bandwidth of a subwavelength plasmonic structure has been observed. Such near-field effects provide new opportunities for the design of ultracompact optical devices, especially wavelength-sensitive devices with subwavelength scales.

Results

Design of the SPP unidirectional coupler. Recently, SPPs attract lots of research interests because of their ability to break the diffraction limit and manipulate light at subwavelength scales[11,12]. They are believed to be promising candidates for constructing the next-generation ultracompact integrated photonic circuits[13]. To realize such

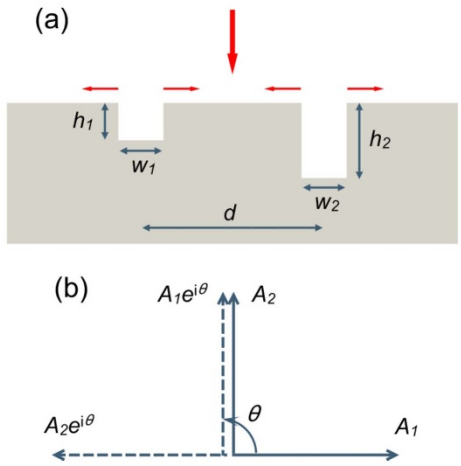

Figure 1 | Schematic diagrams of the groove-doublet structure and the mechanism of SPP unidirectional excitation. (a) The groove-doublet structure with groove widths of w_1 and w_2, groove depths of h_1 and h_2, and the groove separation of d. Under normal incidence, each groove excites two equal SPPs to the left and right directions. (b) Solid vectors (A_1, A_2) represent the directly excited SPPs with equal intensities and an initial phase difference of $\pi/2$ by the two nanogrooves. After propagating over a distance of d, both the two vectors rotate by an angle of $\theta = k_{spp}d$. So, the transmitted SPPs passing through the counterpart grooves can be represented by the two dashed vectors (assuming the transmission coefficients to be 1). If $\theta = \pm\pi/2$, one dashed vector just cancels one solid vector while the other dashed vector interferes with the other solid vector constructively. Thus perfect SPP unidirectional excitation is achieved.

potential, an essential issue is to excite SPPs effectively and to control the direction in which they are launched[6,7,14–23].

A nanogroove with proper dimensions on a metal surface can work as an efficient SPP coupler, when it is resonantly excited by the normal incident light[24,25]. However, the SPP launching intensities to the two opposite directions are equal due to the excitation symmetry. In order to realize unidirectional excitation of SPPs[6,7,14–23], one possible choice is to excite two nanogrooves with different geometries together. Figure 1(a) shows the schematic diagram of the groove-doublet structure, including the geometrical parameters w_1, h_1, w_2, h_2 of the two grooves and the groove separation d. Under normal incidence, each groove excites two equal SPPs to the opposite directions. The complex amplitudes of the excited SPPs by groove 1 and groove 2 are denoted by A_1 and A_2, respectively. The excited SPPs propagating to the counterpart groove will partly transmit through the groove and partly be reflected. The corresponding SPP transmission and reflection coefficients are denoted by t_1, t_2 and r_1, r_2. The finally launched SPP amplitudes away from the groove-doublet to the left A_L and to the right A_R can be expressed as

$$A_L = A_1 + [A_2 \exp(ik_{spp}d) + A_1 r_2 \exp(ik_{spp}\cdot 2d)]t_1 \sum_{n=0}^{+\infty} [r_1 r_2 \exp(ik_{spp}\cdot 2d)]^n \quad (1)$$

$$A_R = A_2 + [A_1 \exp(ik_{spp}d) + A_2 r_1 \exp(ik_{spp}\cdot 2d)]t_2 \sum_{n=0}^{+\infty} [r_2 r_1 \exp(ik_{spp}\cdot 2d)]^n \quad (2)$$

with k_{spp} being the SPP wave vector. Since a nanogroove generally presents a high SPP transmission and a low SPP reflection[26,27], to the zero-order approximation, we can take in account only the first two terms in the right sides of equations (1) and (2) and assume t_1, t_2 to be 1. Then, equations (1) and (2) become

$$A_L = A_1 + A_2 \exp(ik_{spp}d) \quad (3)$$

$$A_R = A_2 + A_1 \exp(ik_{spp}d) \quad (4)$$

Because the groove separation d is small here compared with the SPP propagation length, the SPP propagation loss over such a short distance can be ignored and $\exp(ik_{spp}d)$ mainly represents a pure phase shift factor. Therefore, to achieve the highest contrast between A_L and A_R, we can choose $A_2 = (\pm)i\cdot A_1$ and $\exp(ik_{spp}d) = (\pm)i$. This gives $A_L = 0$ and $A_R = 2A_2$, or $A_L = 2A_1$ and $A_R = 0$, depending on the same signs or the opposite signs are chosen in the brackets. Correspondingly, perfect SPP unidirectional excitation to the right or to the left is obtained with the extinction ratio to infinity. Physically, the above chosen condition means that the two nanogrooves should excite SPPs with equal intensities and an initial phase difference of $\pi/2$ [represented by the solid vectors in Fig. 1(b)]. After propagating over a distance of $d = (n \pm 1/4)\lambda_{spp}$, the transmitted SPPs [represented by the dashed vectors in Fig. 1(b)] are just in phase with the directly excited SPPs in one direction and antiphase in the opposite direction. Consequently, completely constructive interference and destructive interference occur in the according directions.

To test the above proposal, we perform numerical simulations by the finite element method (FEM), using commercial software COMSOL Multiphysics. We start with the SPP excitation property of a single nanogroove at the incident wavelength of $\lambda = 800$ nm. The groove width of $w = 80$ nm (0.1λ) is chosen as a typical example. As the groove depth changes, the SPP excitation shows evident resonant characteristics with the smallest resonant groove depth at 92 nm. According to the previous analysis, two non-resonant groove depths of 67 nm and 134 nm are selected as the working parameters to realize the SPP unidirectional excitation, which provide nearly equal SPP excitation intensities and a phase difference of $\pi/2$ (see Supplementary Fig. S4 online). The scatters in Figs. 2(a) and 2(b) display the FEM-simulated SPP excitation efficiencies of the groove-doublet structure to the left (η_L) and to the right (η_R) as functions of the groove separation d. Here, the SPP excitation efficiency is defined as the SPP power flow to a certain propagation direction normalized by the light power flow incident on the two nanogrooves. As expected, the excited SPPs primarily propagate to the left at groove separations of $d = (n - 1/4)\ \lambda_{spp}$ and to the right at $d = (n + 1/4)\ \lambda_{spp}$. The according extinction ratio η_L/η_R (in dB) is displayed in Fig. 2(c). At $d = (n \pm 1/4)\ \lambda_{spp}$, extinction ratios with high absolute values of about 15 dB are observed. Meanwhile, the SPP excitation efficiency to the unidirectional launching direction is as high as about 1.5. This means the launched SPP power flow is even higher than the incident power flow directly on the two nanogrooves. Thus, efficient unidirectional excitation of SPPs with high extinction ratio as well as high efficiency is successfully realized, which well verifies the previous proposal.

A close examination of Fig. 2(c) reveals that, the extinction ratios at $d = (n \pm 1/4)\ \lambda_{spp}$ are far from infinity which is predicted by the analysis. Such discrepancies can be attributed to the zero-order approximation engaged in the analysis. If we take into account the SPP transmission and reflection effects at the nanogrooves and calculate the SPP excitation efficiencies using equations (1) and (2) (see Methods), we obtain the red lines in Figs. 2(a)–(c). The finite extinction ratios of about 15 dB are well reproduced. This well demonstrates the influence of the SPP scattering property at each groove. To include such effect and achieve nearly perfect extinction of SPPs, we can optimize the structure parameters (see Supplementary Section 2 online). Further FEM simulations show that, by carefully adjusting the groove depths to appropriate values (that is, optimizing A_1 and A_2), the extinction ratios at $d = (n \pm 1/4)\ \lambda_{spp}$ can always reach extremely high values. For instance, at $d = 587$ nm ($3/4\ \lambda_{spp}$), an ultrahigh extinction ratio of about 40 dB is achieved when the groove depths are optimized to $h_1 = 72$ nm and $h_2 = 162$ nm. Figure 2(d)

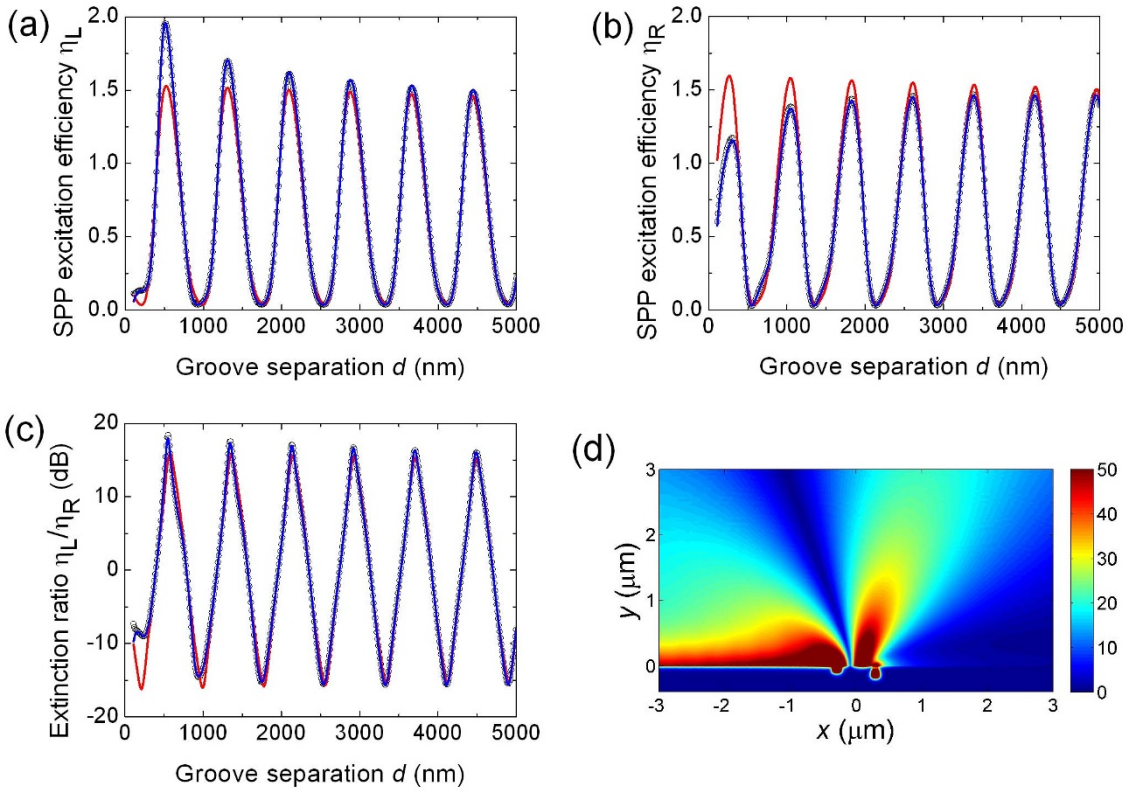

Figure 2 | Unidirectional excitation of SPPs by the groove-doublet structure at incident wavelength of $\lambda = 800$ nm. (a) SPP excitation efficiency to the left (η_L) of the groove-doublet structure (with $w_1 = w_2 = 80$ nm, $h_1 = 67$ nm, $h_2 = 134$ nm) as a function of the groove separation d. (b) SPP excitation efficiency to the right (η_R). (c) According extinction ratio (η_L/η_R) displayed in dB. Scatters show direct FEM simulation results. Red lines indicate calculation results using equations (1) and (2). Blue lines display calculation results using the modified model including CW contributions. (d) The FEM-simulated magnitude of the scattered magnetic field at $d = 587$ nm, with unidirectional launching of SPPs to the left direction clearly seen. The groove depths are optimized to $h_1 = 72$ nm and $h_2 = 162$ nm to achieve a high extinction ratio of about 40 dB (with $w_1 = w_2 = 80$ nm).

presents the FEM-simulated magnitude of the scattered magnetic field, with unidirectional launching of SPPs to the left direction clearly seen.

Bandwidth of the SPP unidirectional coupler. Besides the SPP excitation efficiency and the extinction ratio, the bandwidth is also an important factor for an SPP unidirectional coupler, especially in real applications. Although the extinction ratios at $d = (n \pm 1/4)\,\lambda_{spp}$ can always reach ultrahigh values at a fixed wavelength after optimizing the groove depths, their wavelength dependences are quite different. Roughly speaking, an extinction ratio of ≥10 dB is good enough for many applications. So we define here the bandwidth of an SPP unidirectional coupler as the wavelength range with extinction ratios of ≥10 dB. According to equations (1) and (2), the wavelength response of the proposed SPP unidirectional coupler is mainly determined by two factors. One is the wavelength responses of individual nanogrooves, which does not vary with the groove separation d. The other is the pure interference factor between two interfering sources, which is represented by the propagation phase shift factor $\exp(ik_{spp}d)$. If we ignore the first factor and only take into account the pure interference factor, the zero-order approximation expressions of equations (3) and (4) predict bandwidths of 724, 207, 124, 88 nm at groove separations $d = 1/4\,\lambda_{spp}$, $3/4\,\lambda_{spp}$, $5/4\,\lambda_{spp}$, $7/4\,\lambda_{spp}$. That is, a smaller groove separation gives a broader bandwidth and the bandwidth is roughly inversely proportional to the interference length. This is a common character for the interference between two dispersionless sources. However, the direct FEM simulations show quite different results. The blue, green, orange and red scatters in Fig. 3(a) indicate the FEM-simulated extinction ratios with changing the incident wavelength at groove separations of $d = 1/4\,\lambda_{spp}$, $3/4\,\lambda_{spp}$, $5/4\,\lambda_{spp}$, $7/4\,\lambda_{spp}$. In the simulations, the groove depths are all optimized to ensure nearly perfect extinctions to be achieved at the same central wavelength of $\lambda = 800$ nm. The resulted bandwidths are 107, 174, 127, and 89 nm, respectively. Although the last two bandwidths at $d = 5/4\,\lambda_{spp}$, $7/4\,\lambda_{spp}$ consist well with the previous prediction, the bandwidth at $d = 3/4\,\lambda_{spp}$ is already a little smaller than the predicted value. More seriously, at $d = 1/4\,\lambda_{spp}$, the bandwidth is not only much smaller than the prediction but also evidently smaller than the corresponding bandwidths at $d = 3/4\,\lambda_{spp}$ and $d = 5/4\,\lambda_{spp}$. That is, an abnormal bandwidth shrinking behavior is observed. What is the physical mechanism leading to this anomalous phenomenon? Firstly, we think of the influence of the dispersion effect of the individual grooves, since this fixed factor may have evident impact on the bandwidth at small groove separations [the influence of the pure interference factor $\exp(ik_{spp}d)$ becomes small at small groove separations]. To testify this conception, we make calculations using equations (1), (2) and take into account the wavelength response of each groove (A_1, A_2, t_1, r_1, t_2, r_2 as functions of the wavelength). The calculated bandwidths are 195 nm at $d = 1/4\,\lambda_{spp}$ and 158 nm at $d = 3/4\,\lambda_{spp}$ (in the calculations, the groove depths are also optimized to ensure nearly perfect extinctions to be achieved at $\lambda = 800$ nm). These two bandwidths are evidently smaller than the previous predictions (724 and 207 nm), which clearly demonstrate the influence of the wavelength responses of individual nanogrooves to the bandwidth at small groove separations. The newly calculated bandwidth roughly matches the direct FEM simulation results at $d = 3/4\,\lambda_{spp}$. However, at $d = 1/4\,\lambda_{spp}$, the calculated bandwidth is still significant larger than the FEM simulation result. Besides, the newly calculated bandwidth

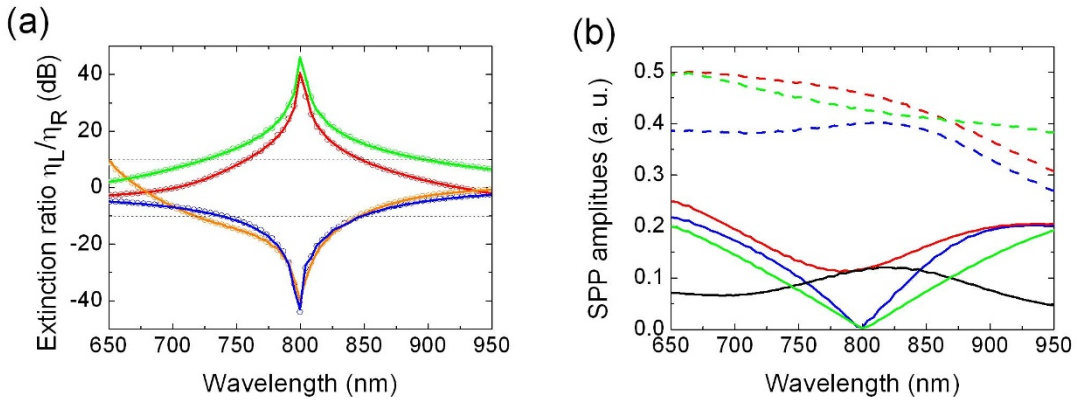

Figure 3 | Wavelength response of the proposed SPP unidirectional coupler and the anomalous bandwidth shrinking behavior at $d = 1/4\ \lambda_{spp}$. (a) Extinction ratios η_L/η_R (in dB) with changing the incident wavelength. Scatters are direct FEM simulation results and lines are calculation results using the modified model including CW contributions. Blue, green, orange and red colors indicate groove separations of $d = 196, 587, 979, 1370$ nm ($1/4\ \lambda_{spp}$, $3/4\ \lambda_{spp}$, $5/4\ \lambda_{spp}$, $7/4\ \lambda_{spp}$), respectively. Groove depths are all optimized by FEM simulations to ensure nearly perfect extinctions at the central wavelength of $\lambda = 800$ nm. (b) Calculated SPP amplitudes $|A_L|$ (solid lines) and $|A_R|$ (dashed lines) at $d = 196$ nm using different models. The wavelength response of η_L/η_R is dominated by $|A_L|$ because the relative change of $|A_L|$ is much bigger than that of $|A_R|$. Red lines display SPP contributions to the total SPP amplitudes coming from the pure SPP model. The black solid line indicates the SPP contribution to $|A_L|$ related to the CW component. This contribution induces an increased wavelength sensitivity of the total SPP amplitude $|A_L|$ (the blue solid line, calculated by the modified model including CW contributions). In contrast, the SPP amplitudes predicted by the pure SPP model are displayed by the green lines (with groove depths optimized to also ensure nearly perfect extinctions at $\lambda = 800$ nm). Without the CW contributions, the SPP amplitudes show much slower variations with the wavelength.

at $d = 1/4\ \lambda_{spp}$ is bigger than that at $d = 3/4\ \lambda_{spp}$. That is to say, these newly calculated bandwidths still fulfill the normal rule. Therefore, the wavelength responses of the two nanogrooves cannot account for the observed abnormal bandwidth shrinking at $d = 1/4\ \lambda_{spp}$.

To get an insight into the anomalous bandwidth shrinking phenomenon, let us recheck Figs. 2(a)–(c) carefully. It is found that the calculated results by equations (1) and (2) deviate from the direct FEM simulation results more and more as the groove separation becomes smaller and smaller. This implies that, except for the propagating SPPs, other near-field effects may also give important contributions. As is known that, in addition to SPPs, quasi-cylindrical waves (CWs) also give evident contributions to the total field on the metal surface at short distances from an electromagnetic source (such as nanogrooves and nanoholes)[28–34]. So, at small groove separations, CWs excited by one groove will be partly scattered into SPPs at the other groove and change the total SPP intensities. To include the CW contribution quantitatively, we employ a modified model which takes into account cross conversions between SPPs and CWs through scatterings at the two nanogrooves (see Methods). The calculated results using this modified model are displayed by the blue lines in Figs. 2(a)–(c). Much better accordance between the calculated results and the direct FEM simulation results is observed compared with the previous pure SPP model based on equations (1) and (2), especially at small groove separations. This means that, although the pure SPP model can demonstrate the main features of the groove-doublet structure, the CW contributions must be considered at small groove separations.

Now we inspect the influence of CWs on the anomalous bandwidth shrinking at $d = 1/4\ \lambda_{spp}$. Using the modified model including CW contributions, the extinction ratios at different wavelengths are calculated and presented by the lines in Fig. 3(a). Nearly perfect match between the calculated results and the direct FEM-simulated results are observed. The anomalous bandwidth shrinking behavior at $d = 1/4\ \lambda_{spp}$ is well reproduced, demonstrating that CWs are responsible for it. To get further into the detailed mechanism, the SPP amplitudes $|A_L|$ and $|A_R|$ at $d = 1/4\ \lambda_{spp}$ are calculated using different models and displayed by the solid and dashed lines in Fig. 3(b). Although the absolute variation with wavelength of $|A_R|$ is comparable to that of $|A_L|$, its relative variation is much smaller due to the much larger absolute value. So the wavelength response of the extinction ratio is mainly determined by the wavelength response of $|A_L|$. The blue solid line shows the calculated $|A_L|$ by the modified model including CW contributions. This total SPP amplitude has two contributions. One coming from the pure SPP model is displayed by the red solid line. The other related to the CW component is indicated by the black solid line. At the best extinction wavelength of $\lambda = 800$ nm, the SPPs contributed by the pure SPP component and the CW component have nearly equal amplitudes and a phase difference of π. They just cancel with each other, resulting in a nearly zero total SPP intensity. When the wavelength deviates from $\lambda = 800$ nm, the SPP amplitude contributed by the pure SPP model [red solid line in Fig. 3(b)] roughly becomes higher and higher. However, the SPPs and the CWs have quite different wavelength-dependent properties due to the dispersion of the metal's permittivity[31]. It turns out that the SPP amplitude contributed by the CWs [black solid line in Fig. 3(b)] roughly becomes lower and lower with the wavelength deviating from $\lambda = 800$ nm. Besides, the phase difference between the SPPs contributed by the pure SPP component and the CW component also deviates from π (for instance, 0.73π at $\lambda = 750$ nm and 1.27π at $\lambda = 850$ nm). Consequently, the SPPs contributed by the pure SPP model are less canceled by the SPPs contributed by the CW component as the wavelength departs from the best extinction position of $\lambda = 800$ nm, and the resulted total SPP amplitude $|A_L|$ is high. Thus, the total SPP amplitude $|A_L|$ changes with the wavelength much rapidly than the SPP amplitude contributed by the pure SPP model. Here, the SPPs contributed by cross conversions between SPPs and CWs increases the variation of the total SPP amplitude $|A_L|$ with changing the wavelength, which in turn decreases the bandwidth. This is the origin of the anomalous bandwidth shrinking behavior at $d = 1/4\ \lambda_{spp}$. For comparison, the SPP amplitudes calculated directly by the pure SPP model (with groove depths optimized to also obtain nearly perfect extinctions at $\lambda = 800$ nm) are displayed by the green line in Fig. 3(b). Without the CW contribution, the SPP amplitude changes with the wavelength much slowly, which gives a broader bandwidth. Thus we get to the conclusion that the bandwidth of the groove-doublet structure at the subwavelength groove separation of $d = 1/4\ \lambda_{spp}$ is significantly reduced by the contribution of the near-field CW component in addition to the

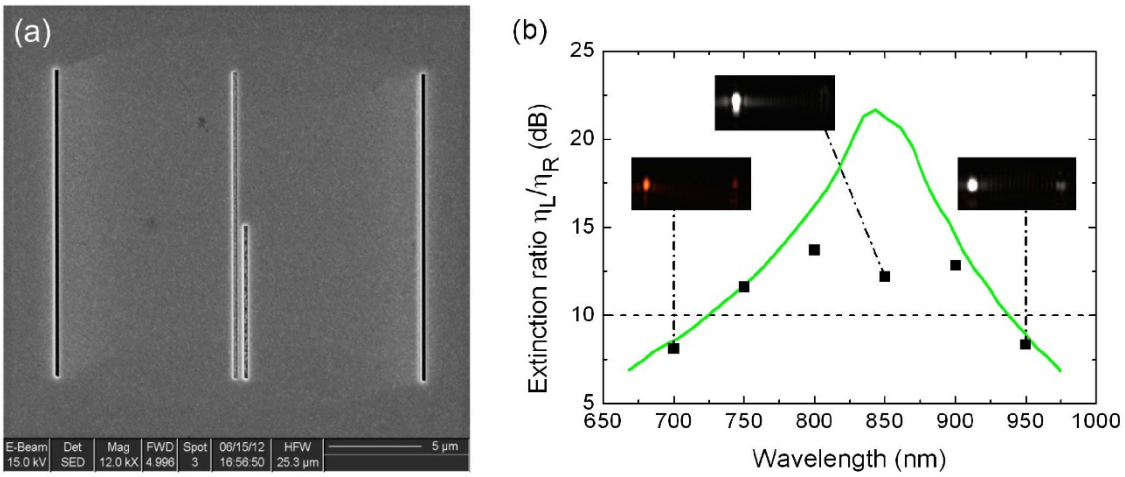

Figure 4 | Experimental demonstration of the broadband SPP unidirectional coupler. (a) SEM image of the experimental structure. In the middle, the groove-doublet is at the lower half and the single nanogroove at the upper half acts as an in-chip reference. Two observation slits cut through the metal film lying symmetrically on the two sides of the groove-doublet with a distance of 10 μm are designed to reconvert the launched SPPs back into photons. The measured geometrical parameters are about $w_1 = 250$ nm, $w_2 = 220$ nm, $h_1 = 100$ nm, $h_2 = 240$ nm, and $d = 565$ nm. (b) Measured extinction ratios η_L/η_R (in dB) at different incident wavelengths are displayed by the scatters, which well match the FEM simulation results displayed by the green line. Insets show typical CCD images with the left-going SPPs clearly seen and the right-going SPPs nearly invisible.

traditional SPP interference effect. (For more details concerning the contributions of different physical mechanisms to the bandwidth of the proposed SPP coupler, see Supplementary Section 3 online.)

Totally speaking, the groove-doublet structure presents the largest bandwidth at groove separation of $d = 3/4\ \lambda_{spp}$. At this working point, an extremely broad bandwidth of 174 nm with high extinction ratios of $\geq$10 dB can be achieved. Meanwhile, the SPP excitation efficiency in the SPP launching direction keeps high values of > 1.15, and the lateral dimension of the whole structure is only about 670 nm. Such a submicron SPP unidirectional coupler with high performance (especially the broad bandwidth) will greatly facilitate the applications.

Experiment. To demonstrate experimentally the proposed SPP unidirectional coupler, we choose bigger groove widths of $w_1 = w_2 = 240$ nm (about 0.3λ) for the sake of easier sample fabrications. FEM simulations show that the proposed SPP unidirectional coupler can work well over a wide range of groove widths if only the groove depths are adjusted accordingly. For the current case, the groove-doublet with $h_1 = 73$ nm and $h_2 = 266$ nm ($w_1 = w_2 = 240$ nm, $d = 587$ nm) presents similar performance as the previous narrow-groove case, with an even little broader bandwidth of about 210 nm.

Experimentally, the groove-doublet structure was fabricated by direct focused ion beam milling in a 450-nm-thick gold film. Figure 4(a) shows a scanning electron microscope (SEM) image of the experimental structure. In the middle, there is a 15-μm-long shallow nanogroove with a 7.5-μm-long deeper nanogroove extended over only the lower half of the shallow nanogroove. Hence, the lower-half structure forms the groove-doublet, while the upper-half single nanogroove acts as an in-chip reference. Two nanoslits cut through the metal film lying symmetrically on the two sides of the central structure with a distance of 10 μm are designed to reconvert the launched SPPs back into photons. So the far-field detected signals can give a direct measurement on the relative intensities of the evanescent SPPs. The measured geometrical parameters are about $w_1 = 250$ nm, $w_2 = 220$ nm, $h_1 = 100$ nm, $h_2 = 240$ nm, and $d = 565$ nm.

In the measurement, the central structure was normally illuminated from the front side using a p-polarized laser beam with a radius of about 3 μm. A fraction of the excited SPPs leaking through the observation slits was collected by an objective from the substrate side and imaged onto a charge coupled device (CCD). Thus, the extinction ratio of the groove-doublet structure could be simply measured by comparing the signal intensities of the two observation slits. Measured results with different incident wavelengths are displayed by the scatters in Fig. 4(b). The bandwidth with extinction ratios of $\geq$10 dB was estimated to be about 200 nm [from 730 to 930 nm, see in Fig. 4(b)]. Typical CCD images displayed in the insets in Fig. 4(b) clearly show the high contrast between the SPPs launched to different directions. The measured extinction ratios well match the FEM simulation results [line in Fig. 4(b)]. Only the extinction ratios with extremely high values are not as high as simulation predictions. This is understandable considering the imperfect sample fabrications, since the sample roughness [see Fig. 4(a), especially in the cavity] will decrease the device performance. This problem may be overcome by using other fabrication techniques which can provide much decreased sample roughness, such as the template stripping method[35,36].

Discussion

Exploiting interference effects is one of the most efficient ways to manipulate light propagation. Traditionally, the bandwidth of an interference component is roughly inversely related to the interference length if the interfering sources have no dispersion effects. Here, we have observed an anomalous bandwidth shrinking phenomenon in the proposed SPP unidirectional coupler when the groove separation is down to a subwavelength scale of $d = 1/4\ \lambda_{spp}$. Calculations show that, the near-field CW component gives important contributions to this abnormal behavior in addition to the interference of propagating SPPs and the dispersion effects of individual grooves. This finding gives the first evidence that the bandwidth of a subwavelength plasmonic structure is significantly affected by the CW component. Although it is a negative factor for the device performance in the current case, CWs actually provide another free degree to manipulate light besides SPPs. With proper designs of the plasmonic structure, CWs may also be utilized to improve the device performance or even realize new functionalities (for instance, to construct subwavelength wavelength-sensitive devices). Such near-field effects provide new opportunities for the design of ultracompact optical devices.

Compared with other existing SPP unidirectional couplers[6,7,14–23], the current design provides simultaneously high efficiency, high

extinction ratio (>40 dB at a specific wavelength) and ultracompact size (lateral dimension about 850 nm). Moreover, it provides an extremely broad bandwidth of >200 nm with high extinction ratios of ≥10 dB. Such broadband nature will greatly facilitate the device's real applications. Another important issue is how much of the total incident light is eventually converted into SPPs. Simulations show that 24% of the total incident light power can be converted into the unidirectional SPPs when the incident Gaussian beam has an optimal beam waist of 600 nm (see Supplementary Section 4 online). Considering the submicron dimension of the proposed SPP unidirectional coupler, this result is rather impressive. Besides, our design also shows high robustness which means a released requirement on sample fabrication accuracy. For instance, if one of the groove width or depth is changed by 10%, FEM simulations show that a broad bandwidth of about 200 nm with high extinction ratios of ≥10 dB can still be maintained and only the central wavelength and the maximal extinction ratio will be changed to a certain extent. That is why good experimental results can be achieved with a relatively rough sample.

Methods

Simulation. Numerical simulations were performed by the finite element method (FEM), using commercial software COMSOL Multiphysics. The permittivity of the gold as a function of the wavelength was taken from literature[37], and expanded using the method of interpolation. For the calculation of equations (1) and (2), the values of t_1, t_2, r_1, r_2 were extracted from FEM simulation results with SPPs incident on a single nanogroove from the left, and the values of A_1, A_2 were extracted from FEM simulation results with Gaussian beam normally incident on a single nanogroove. For the calculations using the modified model including the CW contributions, terms corresponding to CW and SPP cross conversions were added to equations (1) and (2). The calculation of CW and SPP cross conversions follows the strategy in Ref. 32, but with two main differences. One is that not only CW to SPP scattering but also SPP to CW and CW to CW scatterings are included. The other is that the CW component is evaluated by a more rigorous mode decomposition method[31] instead of the simple fitting procedure using equation (1) in Ref. 32.These two differences make the calculations on the current structure more precisely. For more details concerning the implementation of the different calculation models, see Supplementary Section 1 online.

Fabrication. The experimental structure was fabricated using a focused ion beam in a 450-nm-thick gold film. The gold film was evaporated on a glass substrate with a 30-nm-thick titanium adhesion layer.

Measurement. The laser source was a Ti: sapphire laser with the wavelength tunable from 700 nm to 950 nm. The p-polarized (electric field perpendicular to the nanogroove) laser beam was focused to a radius of about 3 μm and normally illuminated the groove-doublet from the front side. Excited SPPs then propagated to the observation slits and partly leaked through to the substrate side. The observation slits were imaged onto a charge coupled device (CCD) by a collecting objective from the substrate side. Typical CCD images displayed in the insets in Fig. 4(b) clearly show the high contrast between the SPPs launched to different directions. For comparison, CCD images obtained when the upper reference single nanogroove was illuminated show similar SPP intensities to different directions. The extinction ratio η_L/η_R of the groove-doublet structure was measured by comparing the signal intensities of the two observation slits (evaluated by integrating over the detected light spots).

1. Born, M. & Wolf, E. *Principles of Optics: Electromagnetic Theory of Propagation, Interference and Diffraction of Light.* (Cambridge University Press, 2001).
2. Balanis, C. A. *Antenna Theory: Analysis and Design.* (John Wiley & Sons, 2005).
3. Mühlschlegel, P., Eisler, H.-J., Martin, O. J. F., Hecht, B. & Pohl, D. W. Resonant optical antennas. *Science* **308**, 1607–1609 (2005).
4. Kosako, T., Kadoya, Y. & Hofmann, H. F. Directional control of light by a nano-optical Yagi–Uda antenna. *Nat. Photon.* **4**, 312–315 (2010).
5. Curto, A. G. *et al.* Unidirectional emission of a quantum dot coupled to a nanoantenna. *Science* **329**, 930–933 (2010).
6. Lerosey, G., Pile, D. F. P., Matheu, P., Bartal, G. & Zhang, X. Controlling the phase and amplitude of plasmon sources at a subwavelength scale. *Nano Lett.* **9**, 327–331 (2009).
7. Liu, Y. *et al.* Compact magnetic antennas for directional excitation of surface plasmons. *Nano Lett.* **12**, 4853–4858 (2012).
8. Liu, Z. *et al.* Focusing surface plasmons with a plasmonic lens. *Nano Lett.* **5**, 1726–1729 (2005).
9. Zhao, C., Wang, J., Wu, X. & Zhang, J. Focusing surface plasmons to multiple focal spots with a launching diffraction grating. *Appl. Phys. Lett.* **94**, 111105 (2009).
10. Evlyukhin, A. B. *et al.* Detuned electrical dipoles for plasmonic sensing. *Nano Lett.* **10**, 4571–4577 (2010).
11. Barnes, W. L., Dereux, A. & Ebbesen, T. W. Surface plasmon subwavelength optics. *Nature* **424**, 824–830 (2003).
12. Gramotnev, D. K. & Bozhevolnyi, S. I. Plasmonics beyond the diffraction limit. *Nat. Photon.* **4**, 83–91 (2010).
13. Ebbesen, T. W., Genet, C. & Bozhevolnyi, S. I. Surface-plasmon circuitry. *Phys. Today* **61**, 44–50 (2008).
14. López-Tejeira, F. *et al.* Efficient unidirectional nanoslit couplers for surface plasmons. *Nat. Phys.* **3**, 324–328 (2007).
15. Bonod, N., Popov, E., Li, L. & Chernov, B. Unidirectional excitation of surface plasmons by slanted gratings. *Opt. Express* **15**, 11427–11432 (2007).
16. Bai, B. *et al.* Asymmetrical excitation of surface plasmon polaritons on blazed gratings at normal incidence. *Phys. Rev. B* **80**, 035407 (2009).
17. Radko, I. P. *et al.* Efficient unidirectional ridge excitation of surface plasmons. *Opt. Express* **17**, 7228–7232 (2009).
18. Roszkiewicz, A. & Nasalski, W. Unidirectional SPP excitation at asymmetrical two-layered metal gratings. *J. Phys. B* **43**, 185401 (2010).
19. Li, X., Tan, Q., Bai, B. & Jin, G. Experimental demonstration of tunable directional excitation of surface plasmon polaritons with a subwavelength metallic double slit. *Appl. Phys. Lett.* **98**, 251109 (2011).
20. Baron, A. *et al.* Compact antenna for efficient and unidirectional launching and decoupling of surface plasmons. *Nano Lett.* **11**, 4207–4212 (2011).
21. Liu, J. S. Q., Pala, R. A., Afshinmanesh, F., Cai, W. S. & Brongersma, M. L. A submicron plasmonic dichroic splitter. *Nat. Commun.* **2**, 525 (2011).
22. Chen, J. J., Li, Z., Yue, S. & Gong, Q. H. Efficient Unidirectional Generation of Surface Plasmon Polaritons with Asymmetric Single-Nanoslit. *Appl. Phys. Lett.* **97**, 041113 (2010).
23. Sonnefraud, Y., Kerman, S., Martino, G. D., Lei, D. Y. & Maier, S. A. Directional excitation of surface plasmon polaritons via nanoslits under varied incidence observed using leakage radiation microscopy. *Opt. Express* **20**, 4893–4902 (2012).
24. Lalanne, P., Hugonin, J. P. & Rodier, J. C. Theory of surface plasmon generation at nanoslit apertures. *Phys. Rev. Lett.* **95**, 263902 (2005).
25. Lalanne, P., Hugonin, J. P. & Rodier, J. C. Approximate model for surface plasmon generation at slit apertures. *J. Opt. Soc. Am. A* **23**, 1608–1615 (2006).
26. Kuttge, M., Abajo, F. J. G. & Polman, A. How grooves reflect and confine surface plasmon polaritons. *Opt. Express* **17**, 10385–10392 (2009).
27. Liu, J. S. Q., White, J. S., Fan, S. & Brongersma, M. L. Side-coupled cavity model for surface plasmon-polariton transmission across a groove. *Opt. Express* **17**, 17837–17848 (2009).
28. Lalanne, P. & Hugonin, J. P. Interaction between optical nano-objects at metallo-dielectric interfaces. *Nat. Phys.* **2**, 551–556 (2006).
29. Liu, H. T. & Lalanne, P. Microscopic theory of the extraordinary optical transmission. *Nature* **452**, 728–731 (2008).
30. Dai, W. & Soukoulis, C. M. Theoretical analysis of the surface wave along a metal-dielectric interface. *Phys. Rev. B* **80**, 155407 (2009).
31. Lalanne, P., Hugonin, J. P., Liu, H. T. & Wang, B. A microscopic view of the electromagnetic properties of sub-λ metallic surfaces. *Surf. Sci. Rep.* **64**, 453–469 (2009).
32. Yang, X. Y., Liu, H. T. & Lalanne, P. Cross conversion between surface plasmon polaritons and quasicylindrical waves. *Phys. Rev. Lett.* **102**, 153903 (2009).
33. Nikitin, A. Y., García-Vidal, F. J. & Martín-Moreno, L. Surface electromagnetic field radiated by a subwavelength hole in a metal film. *Phys. Rev. Lett.* **105**, 073902 (2010).
34. van Beijnum, F. *et al.* Quasi-cylindrical wave contribution in experiments on extraordinary optical transmission. *Nature* **492**, 411–414 (2012).
35. Nagpal, P., Lindquist, N. C., Oh, S. H. & Norris, D. J. Ultrasmooth patterned metals for plasmonics and metamaterials. *Science* **325**, 594–597 (2009).
36. Zhu, X. L. *et al.* Ultrafine and smooth full metal nanostructures for plasmonics. *Adv. Mater.* **22**, 4345–4349 (2010).
37. Johnson, P. B. & Christy, R. W. Optical constants of the noble metals. *Phys. Rev. B* **6**, 4370–4379 (1972).

Acknowledgements

This work was supported by the National Basic Research Program of China (Grants 2009CB930504, 2013CB328704, and 2010CB923200) and the National Natural Science Foundation of China (Grants 11121091, 11134001, and 11204018).

Author contributions

H. L., Z. L. and Q. G. conceived the idea. H. L., Z. L. and J. C. performed simulations and modelling. H. L., Z. L. and X. Z. performed the experiment. S. Y. fabricated the sample. H. L., Z. L. and Q. G. wrote the manuscript together, and all authors reviewed the manuscript.

Additional information

Supplementary information accompanies this paper at http://www.nature.com/scientificreports

Competing financial interests: The authors declare no competing financial interests.

How to cite this article: Liao, H.M. *et al.* A submicron broadband surface-plasmon-polariton unidirectional coupler. *Sci. Rep.* **3**, 1918; DOI:10.1038/srep01918 (2013).